Journal of Asian Earth Sciences 176 (2019) 274–280

Contents lists available at ScienceDirect

Journal of Asian Earth Sciences

journal homepage: www.elsevier.com/locate/jseaes

Full length article

An assessment of present-day crustal deformation in the Kumaun Himalaya from GPS observations

M. Ponraj[a], S. Amirtharaj[a], P.S. Sunil[a,b,*], Ajish P. Saji[a], K. Vijay Kumar[a], S.K. Arora[c], C.D. Reddy[a], S.K. Begum[d]

[a] Indian Institute of Geomagnetism, New Panvel, Navi Mumbai, India
[b] Department of Marine Geology and Geophysics, Cochin University of Science and Technology, Kochi, India
[c] Seismology Division, Bhabha Atomic Research Centre, Mumbai, India
[d] Department of Geophysics, Andhra University, Visakhapatnam, India

ARTICLE INFO

Keywords:
Kumaun Himalaya
Deformation
GPS observations
Slip-rate
Moment deficit
Recurrence interval

ABSTRACT

The India-Eurasia collision has created high mountains in the Himalayan plate boundary system, which has led to numerous earthquakes in this region and released part of the elastic strain accumulated over years. In this study, the present-day deformation pattern is derived from geodetic mode Global Positioning System (GPS) measurements obtained during 2005–2016 from 16 campaign sites in the Kumaun province of the central Himalaya. GPS derived horizontal velocity vectors are in the range of 1–9 mm/yr and 27–38 mm/yr with respect to stable India and Eurasia reference frames respectively. To understand the interseismic strain partitioning in the study region, we consider the uniform slip dislocation model over the fault in an elastic, isotropic and homogeneous half-space medium. The model indicates the Main Himalayan Thrust (MHT) fault is locked to a depth of ~20 km and slips at a rate of 17.2 ± 1 mm/yr with a dip angle of ~7°. This MHT slip rate build-up corresponds to a moment deficit of 8.4 ± 1 × 10^{18} Nm/yr due to locking of the fault beneath the Kumaun Himalaya. The total seismic strain accumulation of 61 × 10^{-6} estimated from the geodetic data suggests the possibility of large earthquakes (typically magnitude 8 and above) with the recurrence interval of around 600 years in the Kumaun Himalayan region.

1. Introduction

The collision between the Indian and Eurasian plates formed the orogenic belt that created the Himalayan mountain arc and Tibetan Plateau. This continental collision led to the elevation of Himalayan-Tibetan topographic features with a combination of crustal thickening and lateral escape (Molnar and Tapponnier, 1975; Harrison et al., 1992; Tapponnier et al., 2001). The structure of the Himalaya is characterized by the underthrusting of the Indian lithosphere beneath the Tibetan Plateau along the Main Himalayan Thrust (MHT) system (Fig. 1) (Zhao et al., 1993). The Himalayan arc longitudinally spans ~2500 km between the western and eastern syntaxes (Molnar and Tapponnier, 1975; Hodges, 2000).

The Indian plate continues to move steadily northward to collide with Eurasia at a convergence rate between 33 and 38 mm/yr from northwest to northeast Himalaya as estimated from GPS observations, and this is reflected in the crustal shortening and shearing in the Himalayan region (Patriat and Achache, 1984; Bilham et al., 1997; Larson et al., 1999; Wang et al., 2001; Zhang et al., 2004; Bettinelli et al., 2006). Crustal shortening results in the formation of major thrust faults namely, the Main Central Thrust (MCT), Main Boundary Thrust (MBT), and Main Frontal Thrust (MFT), as illustrated schematically in Fig. 1 (Gansser 1964; Le Fort, 1975; Nakata, 1989; Yeats et al., 1992). Currently, deformation is mainly accommodated by thrusting across the MHT, which connects the MFT southward to a sub-horizontal single shear zone extending to a depth of 20–30 km below the higher Himalaya (Bollinger et al., 2006; Berger et al., 2004; Lavé and Avouac, 2000). The MFT also bounds the northern limit of the exposed Indian plate and is thought to reach the top of the Indian basement at a depth of about 5 km to extend sub-horizontally beneath the lesser Himalaya along a crustal ramp beneath the frontal part of the higher Himalaya (Pandey et al., 1995; Lavé and Avouac, 2000).

Along the Himalayan arc, in a period of just less than 120 years, the continental collision process has produced three great earthquakes (Fig. 2) that occurred in 1905 (Kangra M_w 7.8), 1934 (Nepal-Bihar M_w 8.1), 1950 (Assam M_w 8.5), and also an earlier earthquake of M_w 7.7 in

* Corresponding author at: Department of Marine Geology and Geophysics, Cochin University of Science and Technology, Kochi, India.
E-mail address: sunilpsiig@gmail.com (P.S. Sunil).

https://doi.org/10.1016/j.jseaes.2019.02.019
Received 28 December 2017; Accepted 5 January 2019
Available online 01 March 2019
1367-9120/

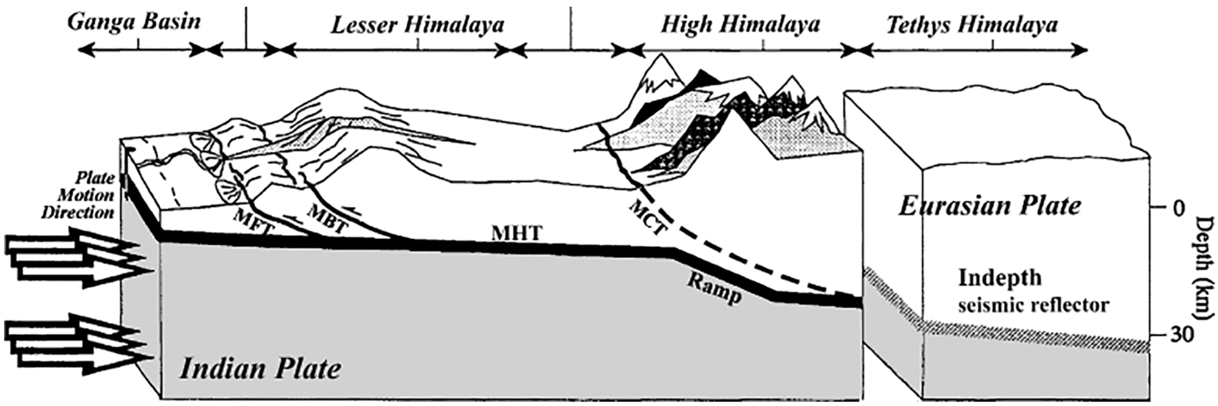

Fig. 1. Schematic representation of the India-Eurasia collision zone and the major fault systems in this zone. MCT: Main Central Thrust; MBT: Main Boundary Thrust; MFT: Main Frontal Thrust. (after Takada and Matsu'ura, 2007).

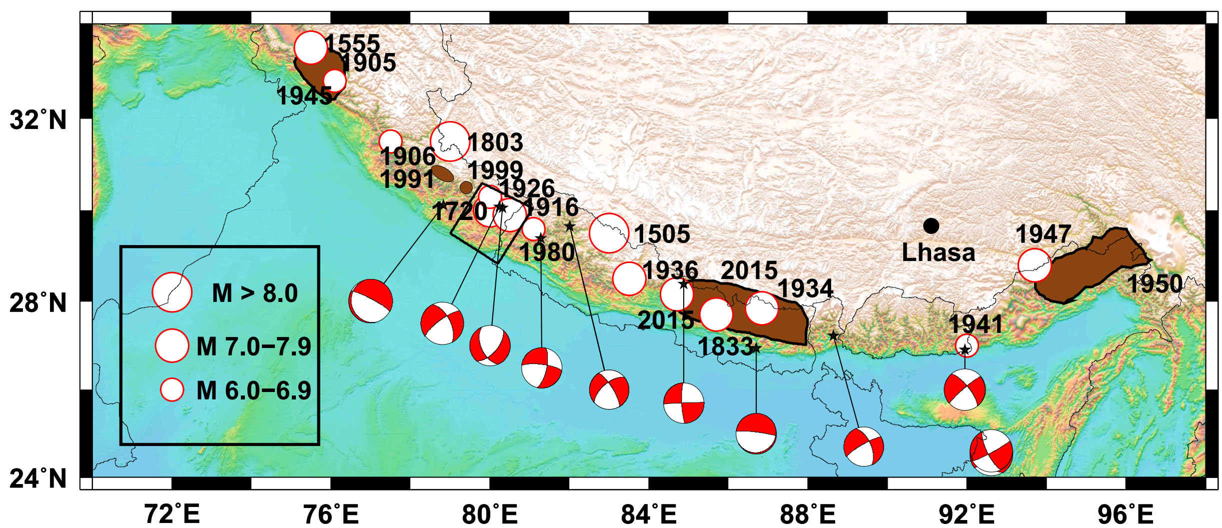

Fig. 2. Epicenters of historical earthquakes (Magnitude M ≥ 6) that occurred along the Himalayan arc are shown as open circles. The size of the circles proportional to their magnitudes, along with the year of their occurrence. The small rectangular area marked in the Himalayan region encloses the the present study area of Kumaun Himalaya. Focal mechanisms of the earthquakes that occurred during the GPS data collection period (2005–2016) are illustrated by beach ball symbols (Harvard CMT data base). The brown shaded areas are the rupture zones of great earthquakes of 1950, 1934 and 1905 (adapted from Kumar et al., 2006; Bilham et al., 2001).

Table 1
GPS-derived horizontal velocities with respect to the India and Eurasia fixed frames. E: East-West component; N: North-South component; σ: Standard deviation.

Site code	Latitude (˚N)	Longitude (˚E)	Velocities in India Fixed Frame				Velocities in Eurasia Fixed Frame			
			East (E) rate mm/yr	North (N) rate mm/yr	σE mm/yr	σN mm/yr	East (E) rate mm/yr	North (N) rate mm/yr	σE mm/yr	σN mm/yr
RAMR	29.395	79.086	−2.06	−1.29	0.67	0.63	5.05	32.55	0.67	0.63
HALD	29.235	79.530	−3.10	−1.67	0.69	0.64	4.22	35.68	0.69	0.64
PILI	28.640	79.820	−1.98	−0.98	0.81	0.71	5.72	33.14	0.81	0.71
BANB	28.996	80.092	−1.99	1.28	0.73	0.65	5.61	35.50	0.73	0.65
PITH	29.587	80.227	−1.94	−0.33	0.0.63	0.60	5.41	33.95	0.0.63	0.60
CHAM	29.336	80.095	−1.39	−0.45	0.77	0.63	6.04	33.77	0.77	0.63
ASKO	29.762	80.336	−0.53	−5.24	0.76	0.63	6.76	29.07	0.76	0.63
DHAR	29.866	80.560	−5.83	−6.93	0.64	0.66	1.48	27.46	0.64	0.66
MUNS	30.064	80.204	−4.36	4.36	0.65	0.60	2.75	38.64	0.65	0.60
GIRG	30.031	80.169	−6.42	−4.67	0.75	0.70	0.69	29.58	0.75	0.70
GWAL	30.002	79.567	−2.36	7.64	1.1	1.2	4.58	41.66	1.1	1.2
GWA2	30.002	79.566	−2.33	7.62	1.4	1.3	4.58	41.66	1.4	1.3
BAGR	29.817	79.775	−3.75	−0.38	0.63	0.58	3.35	33.72	0.63	0.58
KAPK	29.946	79.901	−5.76	−5.46	0.65	0.64	1.32	28.68	0.65	0.64
ALMO	29.590	79.652	−1.39	0.45	0.71	0.64	5.75	34.49	0.71	0.64
NAIN	29.360	79.458	−4.24	4.82	0.66	0.54	2.99	38.80	0.66	0.54
RANI	29.641	79.430	−0.15	−0.16	0.70	0.56	6.94	33.81	0.70	0.56
IISC	13.021	77.570	−3.03	−0.49	0.45	0.53	15.95	34.96	0.45	0.53
HYDE	17.417	78.551	−2.04	−3.18	0.55	0.51	13.53	32.96	0.55	0.51
MUMB	19.133	72.916	−2.93	0.30	0.67	0.61	10.14	32.31	0.67	0.61

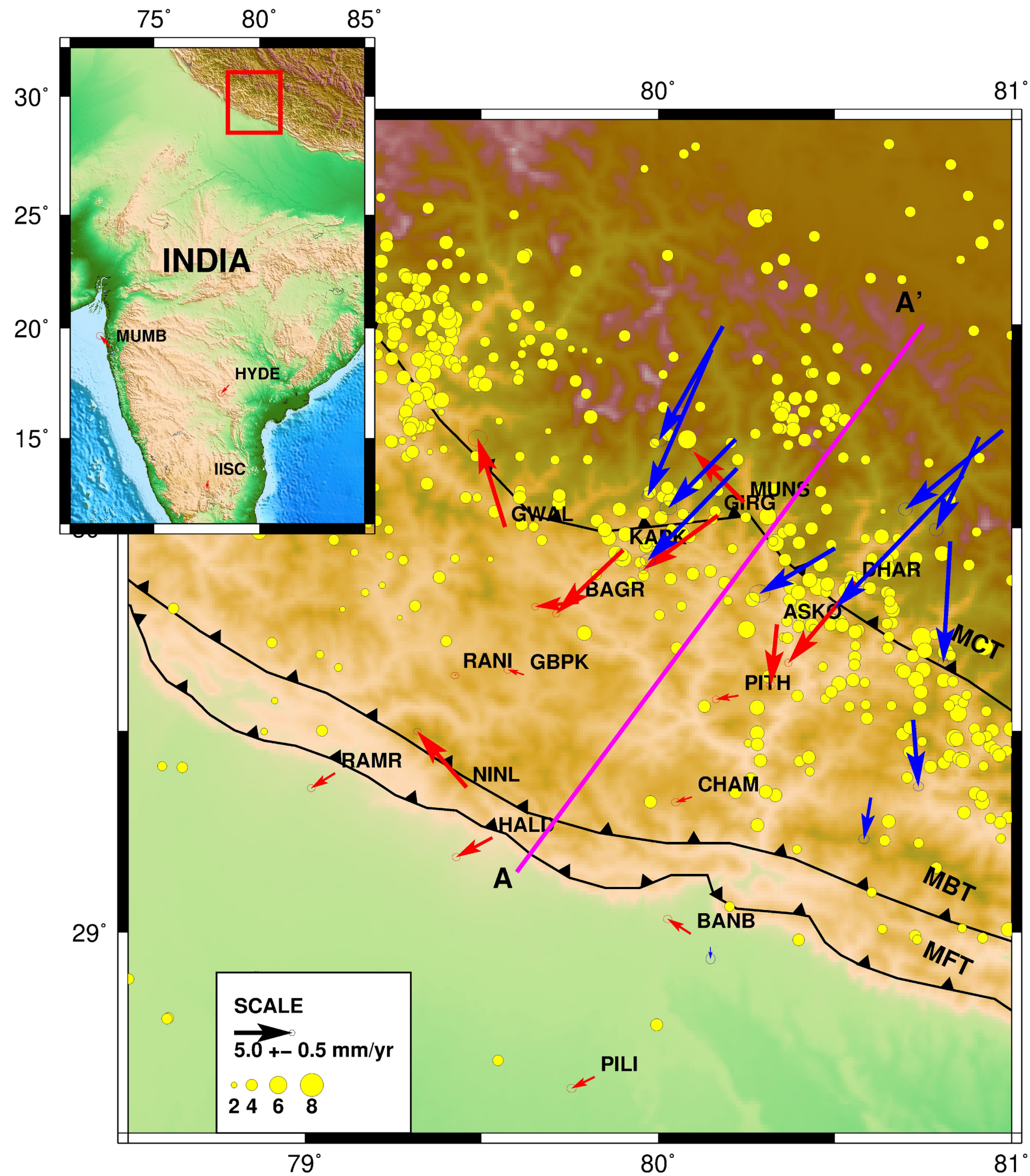

Fig. 3. Central Himalaya seismicity plot (from year 1911 to present, based on the data from International Seismological Centre (ISC) catalogue available at http://www.isc.ac.uk. Estimated GPS site velocities in Indian fixed frame are shown by red arrows. The horizontal velocities considered for the 2-D modelling approach from other studies (Jade et al., 2014; Bettinellli et al., 2006) are represented in blue arrows. The purple line AA' represents the profile along which the estimated velocities are projected in Fig. 4a. The study area is shown as rectangular box in the inset. (For interpretation of the references to colour in this figure legend, the reader is referred to the web version of this article.)

Nepal in 1833 (Seeber and Armbuster, 1981; Molnar and Pandey, 1989, Bollinger et al., 2014). Apart from that, the 1897 (M_w 8.3) earthquake occurred on the Shillong Plateau, south of eastern Himalaya (Bilham and England, 2001; Ambraseys and Douglas 2004). The latest event is the recent Gorkha (Nepal) devastating earthquake (M_w 7.8) that occurred on 25 April 2015 (Avouac et al., 2015; Sreejith et al., 2016). The Kumaun Himalayan region has experienced three large earthquakes of magnitude 7.5 (30.0° N, 80.0° E), 7.3 (29.9° N, 80.5° E) (Ambraseys and Douglas, 2004) and 6.5 (30.3° N, 80.0° E) (Bilham and Ambraseys, 2005) in 1720, 1916 and 1926 respectively. It is evident that the Kumaun region of the lesser Himalaya has not been intensely activated for the past 200 years. Further, the region of the present study lies in the seismic gap between the two great earthquakes (Fig. 2): 1505 (M_w 8.1) and 1803 (M_w 8.2) (Khattri, 1987; Bilham, 1995). Thus, it is conjectured that the Kumaun Himalayan region may exhibit closure of the spatio-temporal seismic gap by producing considerably large

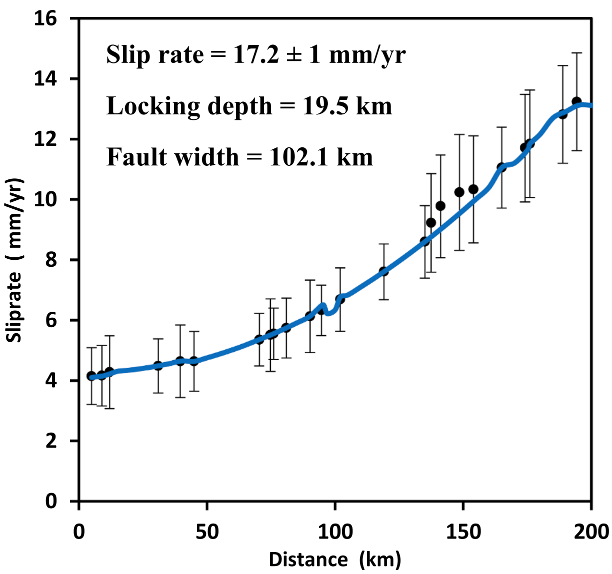

Fig. 4. 2-D Savage dip-slip model of the study area showing (a) N18E projected velocity vs. distance from the MFT along the profile AA' (Fig. 3), (b) observed and calculated velocities, and (c) contours labeled by chi-square distribution in the plot of slip rate vs. MHT fault width; cross symbol in the plot indicates the location of estimated fault parameters (slip rate and fault width).

earthquakes in future. The present study aims to provide insight into the tectonics and geodynamical behavior of the Kumaun Himalaya by investigating the crustal deformation regime through GPS measurements integrated with seismicity.

2. GPS data compilation

The GPS network in the Kumaun Himalaya became operational in campaign mode during May 2005, by establishing a total number of 16 sites. However, the GPS observations commenced in December 2005, and these were repeated annually till 2016 in six epochs (2005–2007, 2009, 2015 and 2016). We preferred winter seasons for all the campaign observations in order to minimize the effect of seasonal variations on the positional error of the GPS sites. The station combination of GPS observations was maintained in all the surveys to reduce the error in determining the station position. All the stations were occupied for 3 to 5 days during each campaign with a sampling interval of 30 s and a cutoff angle of 15°. We analyzed these GPS data together with surrounding International GNSS Service (IGS) fiducial sites (IISC, HYDE, DGAR, SELE, WUHN, LHAZ, BAHR, POL2, KIT3, KUNM, CHUM, SELE, TEHN, URUM and YIBL) employing the GAMIT/GLOBK (King and Bock, 2005; Herring, 2004) post-processing software taking into account the generalized constraints (Dong et al., 1998). We used GPS phase observations obtained every day to estimate station coordinates. The estimated daily GAMIT solutions were refined by minimizing the errors contributed by the receiver and satellite clocks, atmosphere, receiver-phase center variations, phase ambiguities and multipath.

We used the loosely constrained estimates of station coordinates, orbital parameters, and Earth Orientation Parameters (EOP) as well as their associated covariance as quasi-observations which are formed as input to the Kalman filtering part (i.e. GLRED in GLOBK; Herring, 1998) for the estimation of GPS site position time series in International Terrestrial Reference Frame (ITRF) 2008 (Altamimi at al., 2012). Further, to account for longer term errors due to annual and semi- annual tidal effects, we examined the time series (supplementary material) of the daily site positions. We also removed outliers and offsets from the time series, and reweighted the data to overcome the internal inconsistencies arising from large scatter in the data so as to arrive at the systematic trends.

3. GPS data analysis

3.1. Displacements

ITRF-Eurasia Euler pole of Altamimi et al. (2012) (i.e. 56.33° latitude, − 95.979° longitude, and angular velocity of 0.257°/Ma) was used to estimate the velocity of the GPS stations in Eurasia Reference Frame, which is in the range of 27–38 mm/yr (Table 1). The uncertainties in the estimates of horizontal components of velocity are of the order of 1 mm/yr, while those in the vertical component of velocity are ~2.5 mm/yr. The time series (supplementary Fig.S1) for all the stations obtained from all the campaign observations during 2005–2016 in the study region shows a linear trend in the velocity of both the east and north components. This shows the consistency in the Indian plate movement in the northeast direction as well.

In the present study, we employed the ITRF-India Euler pole (Latitude: 51.4°, Longitude: –1.34°, angular velocity of 0.5029°/Ma) determined by Ader et al., (2012), to understand the state of deformation in the study area. The estimated GPS site velocity was converted to the Indian fixed frame by using the same Euler pole. The estimated GPS site velocities are in the range of 1–9 mm/yr. Velocity vectors with respect to the Indian plate are demonstrated in Fig. 3, and the details of which are given in Table 1.

The sites located northeast of MCT are found to have slightly larger motion (blue arrows) compared to those situated southwest of MCT. The deformation gradients seem to have developed between the MCT and the MBT. This suggests that the up-dip portion of the study region is locked. Such a gradient in the velocity across the fault is also observed by GPS measurements in the Nepal Himalaya (Bilham et al., 1997; Larson et al., 1999; Jouanne et al., 1999 and 2004; Sreejith et al., 2018). However, the region where maximum convergence has taken place is far north of the MHT, which tends to accommodate significant shortening (Jouanne et al., 2004) consistent with the geological slip rate over the last few million years (Lavé and Avouac, 2000).

3.2. Modelling approach

The accumulated strain is released periodically through moderate intensity earthquakes in the Himalaya but it does not suffice to release the total budget of the crustal strain (Bilham et al., 1998). Some of the earlier studies (Molnar and Tapponnier, 1975, Larson et al. 1999; Jouanne et al. 1999; Paul et al. 2001; Chen et al. 2004; Bettinelli et al.

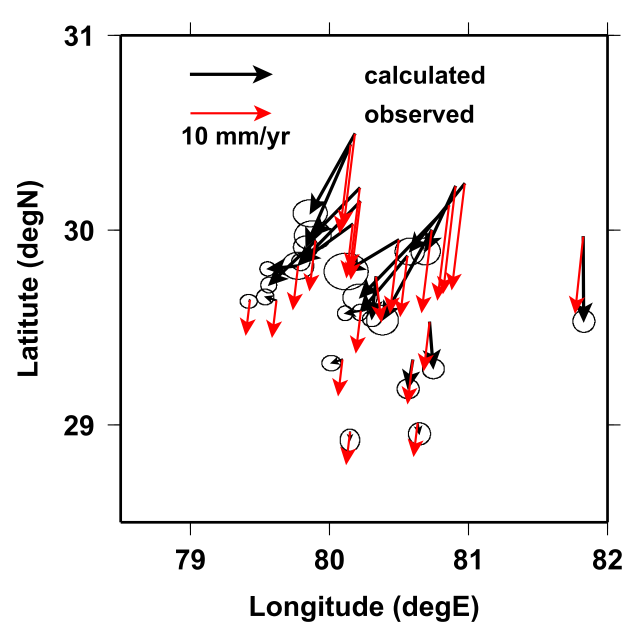

Fig. 4. (*continued*)

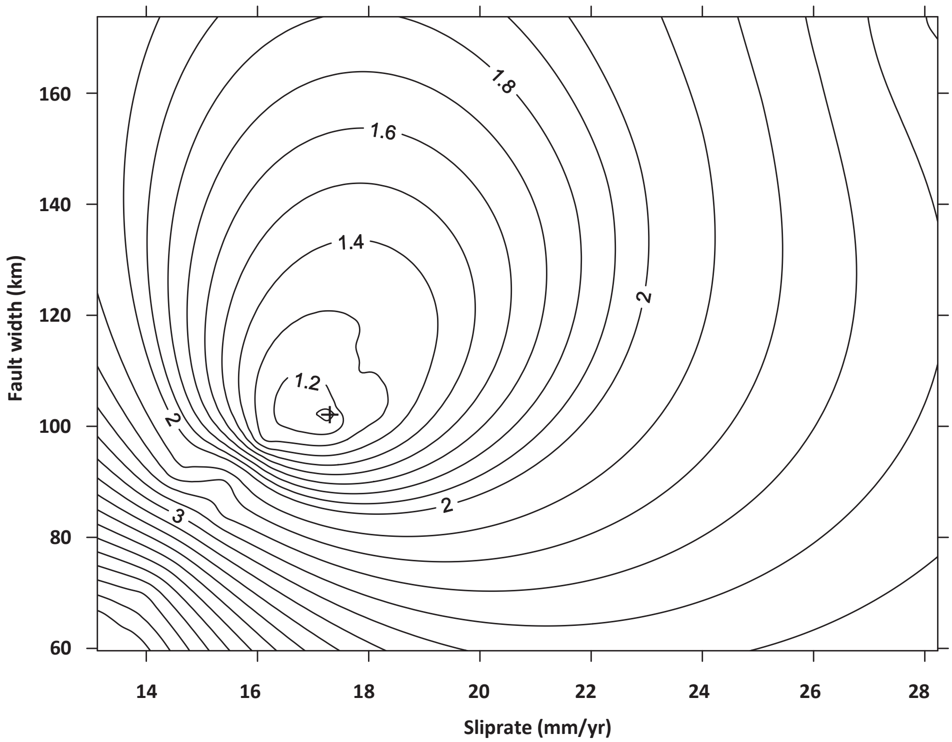

Fig. 4. (*continued*)

2006; Meade, 2007) indicated that a part of the total convergence rate is being absorbed across the Himalaya by slip along the MHT. In the present study, we estimated the slip rate of the MHT across the Kumaun Himalaya by employing the Savage (1983) dip-slip modelling approach.

The slip rate has been estimated by using the GPS derived velocities from the present study, (refer Table.1) published velocities from Bettinelli et al. (2006) (SHB0, DAD2, SHP0, and MAH0) and Jade et al. (2014) (NABH, KALA, GARB, DUNG, MILA, BOGD, LILA, PANG) (please refer Fig. 3 for GPS sites locations). In the modelling approach, the sites in the northeastern part of the MCT are considered as creeping portion of the MHT, whereas the southwestern part is considered as locked.

We determined best-fit GPS site velocity using a varying chi-square method that minimizes the misfit between the observed and calculated velocities. We determined the best-fit values with the dip angles ranging from 5° to 10°. The best-fit value of the locking depth was obtained as ~20 km with fault slip rate of 17.2 ± 1 mm/yr, over a width of ~100 km in a dip angle of 7° (Fig. 4a–c). This model predicts a reasonably close agreement between the observed and calculated velocities (Fig. 4b and c).

4. Discussion

The GPS derived horizontal site velocities show a clear gradient between the MBT to the MCT. The north component clearly brings out the plate convergence, whereas the east component shows the feature of arc-parallel extension. In the study region, we estimated the east-west extension rate as ~13.16 ± 0.5 mm/yr by considering the farthest IGS station located at Lhasa block of Tibetan Plateau as fixed, which is comparable to ~9 mm/yr reported by Jade et al., 2014 and Jade et al., 2017. In substance, the longitudinal extension is construed as a major contributor to the Himalayan arc deformation. The slip-rate estimated from the horizontal velocity vectors indicate a rate of 17.2 ± 1 mm/yr in the Kumaun region of the Himalaya, with a dip angle of ~7° and locking depth of ~20 km (Fig. 4). Earlier GPS studies in the western Nepal Himalaya suggested a slip rate of ~20 mm/yr and locking depth in the range of 12–20 km (Bilham et al., 1997; Jouanne et al., 1999; Larson et al., 1999). The slip rate geologically estimated by Wesnousky et al., (1999) in the Nepal Himalaya is 13.8 ± 3.6 mm/yr, and that in the Western Himalaya is ~15 mm/yr with a locking depth of 15 km (Banerjee and Bürgmann, 2002).

4.1. Moment rate

Seismic moment rate ($\dot{M}_0$) is defined as the product of the study area (100 km × 150 km) and the slip rate (17 mm/yr) (Maruyama, 1963; Brune, 1968). In earlier studies, the moment deficit rate in the Nepal Himalaya over a locking depth range of 15–20 km is reported as ~6.6 × 10^{19} N-m/yr (Ader et al., 2012), and ~15 × 10^{19} N-m/yr (Stevens and Avouac, 2015) for the entire Himalayan arc. In the present study, using the standard empirical relation (Brune, 1968), the moment deficit rate is obtained as 8.4 ± 1 × 10^{18} N-m/yr.

The seismic moment rate (M_0^s) of each of the earthquake events with moment magnitudes (M_w) above 3.0 is estimated using the following empirical relation (Kanamori, 1977).

$$M_0^s = 10^{(1.5M_w+16.095)} \times 10^{-7} N - m \quad (1)$$

According to Rundle (1989), the geodetic moment released in the resulting earthquakes obeys the distribution law:

$$N(M_0) = \alpha M_0^{-\beta} \quad (2)$$

where N is the number of earthquakes of moment ≥M_0 and α and β are some constants; α depends on the rate of earthquake activity, whereas β represents the seismic severity governed by the relative numbers of large and small earthquakes. The largest earthquake event with its moment denoted by M_0^{max} is so specified as to keep the total seismic moment finite. The ratio of the maximum seismic moment (M_0^{max}) to the moment rate ($\dot{M}_0$) during a time interval T corresponding to the average repeat time of the largest earthquake is approximately 1-β (McCaffrey et al., 2000). Hence, the total moment released during the time T equals $T\dot{M}_0$ which is the same as $M_0^{max}/(1\text{-}\beta)$. This is consistent with the following expression:

$$T = M_0^{max}/(1-\beta)\dot{M}_0 \quad (3)$$

We employed the above expression (3) to determine the return period of a typically large earthquake of moment magnitude $M_w = 8$. For such a great earthquake, the computed value of M_0^{max} is 1.2×10^{21} N-m, and the corresponding elastic strain accumulation is 61×10^{-6} strain, assuming a typical value of β at 0.76 as suggested by Kagan (1997), applicable to India-Tibet seismic zone that encompasses our study area. Taking into account all these parametric values, it turns out that a time interval of approximately 600 years is adequate to generate the assumed 8.0 magnitude earthquake in the Kumaun Himalayan region. Feldl and Bilham (2006) estimated that, in central Himalaya, an earthquake of moment magnitude at least 8.6 would tend to repeat with an interval of ~500 yrs.

5. Conclusion

Seismotectonic activity in the Kumaun Himalaya is analyzed using geodetic data obtained from campaign mode GPS observations. The velocities of GPS sites are found to be in the range of 1–9 mm/yr and 27–38 mm/yr with respect to India and Eurasia fixed reference frames respectively. The 2-D model suggests that the MHT slip rate in the Kumaun Himalayan region is building up at ~17 mm/yr with a dip angle of ~7° and a locking depth of ~20 km. The study from the geodetic data reveals the total accumulation of seismic strain in the order of 61×10^{-6}, which would be enough to generate an earthquake of magnitude 8 with a recurrence interval of about 600 years in the Kumaun Himalayan province.

Acknowledgements

We thank Director, Indian Institute of Geomagnetism for his constant encouragement and support during this study. Our sincere thanks to K. Deenadayalan for his assistance at different stage of manuscript preparation. We thank Robert W King for the GAMIT/GLOBK GPS data analysis software. Our sincere thanks to the anonymous reviewers for their critical comments and suggestions which helped to improve the manuscript. Figures were generated with the help of Generic Mapping Tools (GMT).

Appendix A. Supplementary material

Supplementary data to this article can be found online at https://doi.org/10.1016/j.jseaes.2019.02.019.

References

Ader, T., Avouac, J.-P., Jing, L.-Z., Hèlène, L.-C., Bollinger, L., Galetzka, J., Genrich, J., Thomas, M., Chanard, K., Sapkota, S.N., Rajaure, S., Shrestha, P., Ding, L., Flouzat, M., 2012. Convergence rate across the Nepal Himalaya and interseismic coupling on the main himalayan thrust, implications for seismic hazard. J. Geophys. Res. 117, B04403. https://doi.org/10.1029/2011JB009071.
Altamimi, Z., Métivier, L., Collilieux, X., 2012. ITRF 2008 plate motion model. J. Geophys. Res. 117, B07402. https://doi.org/10.1029/2011JB0089302214.
Ambraseys, N.N., Douglas, J., 2004. Magnitude calibration of north Indian earthquakes. Geophys. J. Int. 158, 1–42.
Avouac, J.-P., Meng, L., Wei, S., Wang, T., Ampuero, J.-P., 2015. Lower edge of locked Main Himalayan Thrust unzipped by the 2015 Gorkha earthquake. Natural Geosci. 8, 708–711.
Banerjee, P., Bürgmann, R., 2002. Convergence across northwest Himalaya from GPS measurements. Geophys. Res. Lett. 29 (13), 301–304.
Berger, A., Jouanne, F., Hassani, R., Mugnier, J.L., 2004. Modelling the spatial distribution of present day deformationin Nepal, how cylindricall is the Main Himalayan Thrust in Nepal? Geophys. J. Int. 156, 94–114.
Bettinelli, P., Avouac, J.-P., Flouzat, M., Jouanne, F., Bollinger, L., Willis, P., Chitraker, G.R., 2006. Plate motion of India and interseismic strain in the Nepal Himalaya from GPS and Doris measurements. J. Geod. https://doi.org/10.1007/s00190-006-0030-3.
Bilham, R., 1995. Location and magnitude of the 1833 Nepal earthquake and its relation to the rupture zones of contiguous great Himalayan earthquakes. Curr. Sci. 69 (2), 155–187.
Bilham, R., Blume, F., Bendick, R., Gaur, V.K., 1998. Geodetic constraints on the translation and deformation of India: implications for future great Himalayan earthquakes. Curr. Sci. 74, 213–229.
Bilham, R., Ambraseys, N., 2005. Apparent Himalayan slip deficit from the summation of seismic moments for Himalayan earthquakes 1500–2000. Curr. Sci. 88 (10), 1658–1663.
Biham, R., England, P., 2001. Plateau pop-up during the 1897 Assam earthquake. Earth Scicences Oxford University, UK.
Bilham, R., Gaur, V.K., Molnar, P., 2001. Himalayan Seismic Hazard. Science 293, 14421–14444.
Bilham, R., Larson, K., Freymueller, J.T., Project Idylhim members, 1997. GPS measurements of present-day convergence across the Nepal Himalaya. Nature 386, 61–64.
Bollinger, L., Sapkota, S.N., Tapponnier, P., Klinger, Y., Rizza, M., Van der Woerd, J., Tiwari, D.R., Pandey, R., Bitri, A., Bes de Berc, S., 2014. Estimating the return times of great Himalayan earthquakes in eastern Nepal, evidence from the patu and bardibas strands of the main frontal thrust. J. Geophys. Res. 119. https://doi.org/10.1002/2014JB010970.
Bollinger, L., Henry, P., Avouac, J.-P., 2006. Mountain building in the Nepal Himalaya, thermal and kinematic model. Earth Planet Science Letters 244, 58–71.
Brune, J.N., 1968. Seismic moment, seismicity, and rate of slip along major fault zones. J. Geophys. Res. 73, 777–784. https://doi.org/10.1029/JB073i002p00777.
Chen, Q., Freymueller, J.T., Wang, Q., Yang, Z., Xu, C., Jiang, W., Wang, Q., Liu, J., 2004. Spatially variable extension in southern Tibet based on GPS measurements. J. Geophys. Res. 109, B09401. https://doi.org/10.1029/2002JB002350.
Dong, D., Herring, T.A., King, R.W., 1998. Estimating regional deformation from a combination of space and terrestrial geodetic data. J. Geod. 72, 200–211.
Feldl, N., Bilham, R., 2006. Great Himalayan earthquakes and the Tibetan Plateau. Nature 444, 165–170.
Gansser, A., 1964. Geology of the Himalayas. Interscience, London.
Harrison, T.M., Copeland, P., Kidd, W.S.F., Yin, A., 1992. Raising Tibet. Science 255, 1663–1670.
Herring, T.A., 1998. GLOBK. Global Kalman filter VLBI and GPS analysis program Version 3.2 Internal Memorandum. Massachusetts Institute of Technology, Cambridge 1998.
Herring, T.A., 2004. Global Kalman Filter VLBI and GPS Analysis Program Version 4.1. Mass. Inst Tech, Cambridge.
Hodges, K.V., 2000. Tectonics of the Himalaya and Tibet from two perspectives. Geolog. Soc. American Bulletin 112, 324–350.
http://www.isc.ac.uk, International Seis. Cent., Thatcham, United Kingdom, 2013.
Jade, S., Mukul, M., Gaur, V.K., Kumar, K., Shrungeshwar, T.S., Satyal, G.S., Dumka, R.K., Jagannathan, S., Ananda, M.B., Dileep Kumar, P., Banerjee, S., 2014. Contemporary deformation in the Kashmir-Himachal, Garhwal and Kumaon Himalaya, significant insights from 1995–2008 GPS time series. J. Geod. 88, 539–557.
Jade, S., Shrungeshwara, T.S., Kumar, K., Choudhury, P., Dumka, R.K., Bhu, H., 2017. India plate angular velocity and contemporary deformation rates from continuous GPS measurements from 1996 to 2015. Sci. Rep. 7, 11439. https://doi.org/10.1038/s41598-017-11697-w.
Jouanne, F., Mugnier, J.L., Pandey, M.R., Gamond, J.F., Le Fort, P., Serrurier, P., Vigny, C., Avouac, J.-P., Idylhim members, 1999. Oblique convergence in Himalaya of western Nepal deduced from preliminary results of GPS measurements. Geophys. Res. Lett. 26, 1933–1936.
Jouanne, F., Mugnier, J.L., Gamond, J.F., Le Fort, P., Pandey, M.R., Bollinger, L., Flouzat, M., Avouac, J.-P., 2004. Current shortening across the Himalayas of Nepal. Geophys. J. Int. 157, 1–14.
Kagan, Y.Y., 1997. Seismic moment-frequency relation for shallow earthquakes, Regional comparison. J. Geophys. Res. 88, 2835–2852.
Kanamori, H., 1977. The energy release in great earthquakes. J. Geophys. Res. 82, 2981–2987.
Khattri, K.N., 1987. Great earthquakes, seismicity gaps and potential for earthquakes along the Himalayan plate boundary. Tectonophysics 38, 79–92.
King, R.W., Bock, Y., 2005. Documentation of the GAMIT GPS Analysis Software. Mass. Inst. Of Technol, Massachusetts.
Kumar, S., Wesnousky, S.G., Rockwell, T.K., Briggs, R.W., Thakur, V.C., Perumal, R.J., 2006. Paleoseismic evidence of great surface rupture earthquakes along the Indian Himalaya. J. Geophys. Res. 111, B03304. https://doi.org/10.1029/2004JB003309.
Larson, K.M., Burgmann, R., Bilham, R., Freymueller, J.T., 1999. Kinematics of the India-Eurasia collision zone from GPS measurements. J. Geophys. Res. 104, 1077–1093.
Lav'e, J., Avouac, J.P., 2000. Active folding of fluvial terraces across the Siwaliks Hills, Himalayas of central Nepal. J. Geophys. Res. 105, 5735–5770.
Le Fort, P., 1975. Himalaya, the collided range; present knowledge of the continental arc. Am. J. Sci. 275A, 1–44.
Maruyama, T., 1963. On the Force Equivalent of Dynamic Elastic Dislocations with Reference to the Earthquake Mechanism. Bulletin Earthquake Research Instittue, Tokyo University, pp. p467.
McCaffrey, R., Long, M.D., Goldfinger, C., Zwick, P.C., Nabelek, J.L., Johnson, C.K., Smith, C., 2000. Rotation and plate locking at the southern Cascadia subduction zone. Geophys. Res. Lett. 27, 3117–3120.
Meade, B.J., 2007. Present-day kinematics at the India-Asia collision zone. Geology 35 (1), 81–84. https://doi.org/10.1130/G22924A.1.
Molnar, P., Pandey, M.R., 1989. Rupture zones of Great Earthquakes in the Himalayan region. Proceedings of Indian Academy of Science, pp. 61–70.
Molnar, P., Tapponnier, P., 1975. Cenozoic tectonics of Asia, Effects of a continental collision. Science 189, 419–426.
Nakata, T., 1989. Active faults of the Himalayas of India and Nepal. Geolog. Soc. American Bulletin 232, 243–264.
Pandey, M.R., Tandukar, R.P., Avouac, J.-P., Lavè, J., Assot, J.P., 1995. Interseismic strain accumulation on the Himalaya crustal ramp (Nepal). Geophys. Res. Lett. 22, 741–754.
Patriat, P., Achache, J., 1984. India-Eurasia collision chronology has implications for crustal shortening and driving mechanism of plates. Nature 311, 615–621.

Paul, J., Bürgmann, R., Gaur, V.K., Bilham, R., Larson, K., Ananda, M.B., Jade, S., Mukul, M., Anupama, T.S., Satyal, G., Kumar, D., 2001. The motion and active deformation of India. Geophys. Res. Lett. 28, 647–651.

Rundle, B.J., 1989. Derivation of the complete Gutenberg-Richter magnitude-frequency relation using the principle of scale invariance. J. Geophys. Res. 94, 12337–12342.

Savage, J.C., 1983. A dislocation model of strain accumulation and release at a subduction zone. J. Geophys. Res. 88, 4984–4996.

Seeber, L., Armbruster, J.G., 1981. Great detachment earthquakes along the Himalayan Arc and long term forecasting, Earthquake Prediction, An International Review. Maurice Ewing Series vol. 4, Edited by D.W. Simpson and P. G. Richards, AGU, 259–277.

Sreejith, K.M., Sunil, P.S., Agrawal, R., Saji, A.P., Ramesh, D.S., Rajawat, A.S., 2016. Coseismic and early postseismic deformation due to the 25 April 2015, M_w 7.8 Gorkha, Nepal earthquake from InSAR and GPS measurements. Geophysical Res. Lett. https://doi.org/10.1002/2016GL067907.

Sreejith, K.M., Sunil, P.S., Agrawal, R., Saji, A.P., Rajawat, A.S., Ramesh, D.S., 2018. Audit of stored strain energy and extent of future earthquake rupture in central Himalaya. Sci. Rep. 8, 16697. https://doi.org/10.1038/s41598-018-35025-y.

Stevens, S.L., Avouac, J.-P., 2015. Interseismic coupling on the main Himlayan thrust. Geophys. Res. Lett. 42. https://doi.org/10.1002/2015GL064845.

Takada, Y., Matsu'ura, M., 2007. Geometric evolution of a plate interface–branch fault system: Its effects on the tectonic development of the Himalayas. J. Asian Earth Sci. 29, 490–503.

Tapponnier, P., Xu, Z.Q., Roger, F., Meyer, B., Arnaud, N., Wittlinger, G., Yang, J.S., 2001. Oblique step wise rise and growth of the Tibet plateau. Science 294 (5547), 1671–1677.

Wang, Q., Zhang, P.-Z., Freymueller, J.T., Bilham, R., Larson, K.M., Lai, X., You, X., Niu, Z., Wu, J., Li, Y., Liu, J., Yang, Z., Chen, Q., 2001. Present-day crustal deformation in China constrained by Global Positioning System measurements. Science 295, 574–577.

Wesnousky, S.G., Senthil, K., Mohindra, R., Thakur, V.C., 1999. Uplift and convergence along the Himalayan Frontal Thrust of India. Tectonics 18 (6), 967–976.

Yeats, R.S., Nakata, T., Farah, A., Mizra, M.A., Pandey, M.R., Stein, R.S., 1992. The Himalayan frontal fault system. Annales Tectonicae, Special Issue 6, 85–98.

Zhang, P., Shen, Z., Wang, M., Gan, W., Bürgmann, R., Molnar, P., 2004. Continuous deformation of the Tibetan Plateau from global positioning system data. Geology 32, 809–812.

Zhao, W., Nelson, K.D., project INDEPTH Team, 1993. Deep seismic-reflection evidence continental under thrusting beneath southern Tibet. Nature 366, 557–559.